ACADEMIC PRESS

Available online at www.sciencedirect.com

SCIENCE DIRECT®

Journal of Molecular Spectroscopy 219 (2003) 263–270

Journal of MOLECULAR SPECTROSCOPY

www.elsevier.com/locate/jms

Rotational analysis of the (3,3) and (4,4) bands of the $A^2\Pi_u \leftarrow X^2\Sigma_g^+$ system of N_2^+ in the near-infrared using velocity modulation spectroscopy

Christopher G. Tarsitano* and Takeshi Oka

Department of Chemistry, University of Chicago, Chicago, IL, USA
Department of Astronomy and Astrophysics, University of Chicago, Chicago, IL, USA
The Enrico Fermi Institute, University of Chicago, Chicago, IL, USA

Received 25 September 2002

Abstract

The (3,3) and (4,4) bands of the $A^2\Pi_u \leftarrow X^2\Sigma_g^+$ system of N_2^+ has been studied using the velocity modulation technique in the near-infrared region. The rotational structure has been analyzed by the method of combination differences in conjuction with the standard Hamiltonian. Molecular parameters and rotational temperatures are reported.
© 2003 Elsevier Science (USA). All rights reserved.

PACS: 33.15.-e; 33.20.-t; 33.20.Ea

Keywords: N_2^+; Near-infrared; Spectroscopy; Absorption

1. Introduction

In 1932, Childs predicted that a lower lying Π state was causing the observed perturbations in the *B*–*X* system of N_2^+ [1]. The perturbing state was found 18 years later, in 1950, when Meinel observed a new spectrum in an auroral emission in the near-infrared [2,3]. The $A^2\Pi_u \leftarrow X^2\Sigma_g^+$ system is now called the Meinel system. Soon afterwards, the first laboratory spectrum of the Meinel system was obtained by Dalby and Douglas [4] and Douglas [5]. In 1980, Benesch, Rivers, and Moore measured in emission eight bands of the Meinel system [6]. These bands were later analyzed by Miller et al. [7] when the bands were fit to a model Hamiltonian together with their (4,0) band obtained by LIF spectroscopy.

Since then, many spectroscopists have studied the Meinel system. One useful technique in the study of molecular ions is the velocity modulation technique, developed by Gudeman, Saykally, and others [8,9]. This technique has been applied extensively to the $A^2\Pi_u \leftarrow X^2\Sigma_g^+$ system of N_2^+ [10–20]. This paper reports on the observation of two new bands of the Meinel system, the (3,3) and (4,4) bands, using velocity modulation spectroscopy.

2. Experimental

A computer-controlled New Focus external-cavity tunable diode laser supplied the near-infrared radiation. The diode laser has been used earlier for the observation of the combination bands of H_3^+ [21]. The experimental setup, shown in Fig. 1, differed from the previous experiment in detail. The laser can be tuned over the wavelength range 1222–1300 nm, with a single-mode output power on the order of several milliwatts and a linewidth less than 300 kHz. Scanning of the computer-controlled laser is accomplished by (a) stepping up a picomotor for coarse wavelength control and (b) changing the voltage on a piezoelectric transducer for fine frequency control. The resulting spectra consisted of a series of 60 GHz fine frequency controlled segments that partially overlap one another. Each 60 GHz segment

* Corresponding author.
E-mail address: tarsitan@fermi.uchicago.edu (C.G. Tarsitano).

0022-2852/03/$ - see front matter © 2003 Elsevier Science (USA). All rights reserved.
doi:10.1016/S0022-2852(03)00012-2

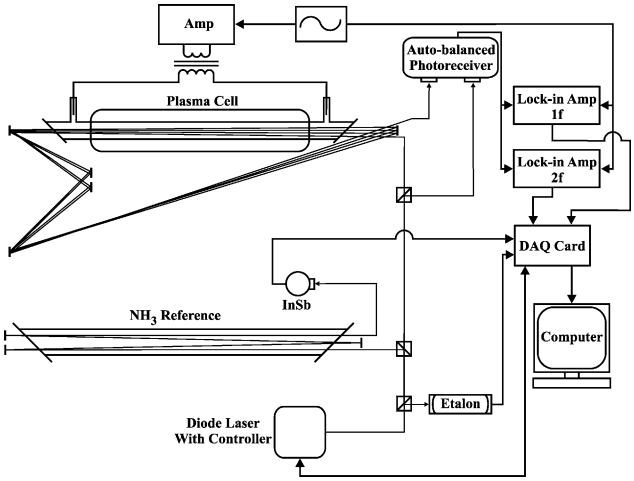

Fig. 1. Schematic diagram for the velocity modulation diode laser spectrometer.

contained 2000 data points, where each data point is separated by approximately 30 MHz. Additionally, each datapoint consisted of a computer average of 20 samples.

The N_2^+ molecular ions were produced in a liquid nitrogen-cooled positive column discharge as described in [22]. In brief, the reagent gases (7 Torr helium and 0.2 Torr N_2) flowed into the discharge cell through 18 inlets and pumped out by a mechanical pump through 9 outlets. The bore of the discharge tube had a length of approximately 1.35 m and an inner diameter of 1.2 cm. The plasma was produced by supplying a 19 kHz ac potential, on the order of several kilovolts, to the electrodes located at each side and off axis to the discharge tube. The resulting discharge current was approximately 75 mA (rms).

The laser output was split into two beams, one reference and one signal beam, for subtraction of the amplitude noise of the laser. The signal beam passed through the discharge cell in a modified white cell configuration such that four unidirectional passes were obtained resulting in a total path length of approximately 5.4 m. A New Focus Nirvana auto-balanced photoreceiver was used to simultaneously detect both the reference and signal beams. The noise-subtracted absorption signal was demodulated at 1f and 2f using a Stanford Research Systems SR510 lock-in amplifiers. The time constant of the lock-in amplifiers and the scanning rate of the laser were optimized by repeatedly scanning over an N_2^+ line and monitoring the line such that there were no distortions to the line shape or shifts in the frequency of the line. It was found that the optimal settings for the time constant and the scanning rate were 0.1 ms and approximately 480 MHz/s, respectively.

The absorption spectra of the overtone bands of NH_3 and the transmission of a 2 GHz etalon were simultaneously recorded to provide both absolute and relative wavenumber calibration. The NH_3 spectra were recorded using a pressure of approximately 7 Torr of NH_3. The laser beam was multipassed 16 times in a white cell configuration to produce a total path length of about 32 m. To account for thermal fluctuations of the etalon, two NH_3 absorption lines were used to determine the spacing between etalon fringes in a segment. When only one NH_3 line was present in a segment, the average value for the spacing between etalon ticks was used. The FTIR NH_3 spectra, kindly provided by G. Guelachvili, that has an overall accuracy of $\pm 0.002\ cm^{-1}$ in this region was used [23]. The absolute accuracy of the line position measurements in our spectrum is believed to be better than $0.005\ cm^{-1}$.

3. Results

The Doppler-limited spectra of the (3,3) and (4,4) vibrational bands of the A–X system of N_2^+ were recorded over the entire diode range between 7691.1 and $8178.6\ cm^{-1}$. The velocity modulated absorption lines were fit to a first derivative Gaussian. Overlapped lines were fit to a function that consisted of multiple first derivative Gaussians. Fig. 2 shows a portion of the spectrum of the (4,4) vibrational band of the A–X system.

The rotational analysis of the bands was straightforward. The standard Hund's case (b) Hamiltonian was used for modeling the ground $^2\Sigma_g^+$ state, which consisted of the molecular parameters T_v, B_v, D_v, and γ_v, the electronic and vibrational energy, the rotational constant, the quartic centrifugal distortion constant, and the spin-rotation constant, respectively. The excited state was modeled using the $^2\Pi$ Hamiltonian described by Endo et al. [24] which consisted of the spin–orbit

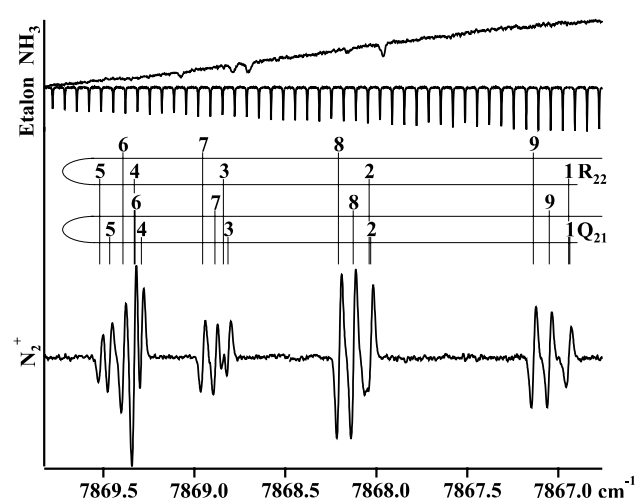

Fig. 2. Sample spectrum of the (4,4) band of the $A^2\Pi_u \leftarrow X^2\Sigma_g^+$ system of N_2^+ showing bandhead formation, the evolution of the spin-rotation splitting, and the intensity alteration as a result of the nuclear spin statistics in the R_{22} and Q_{21} subbands.

Table 1
Wavenumbers of the observed lines of the (3,3) band of the $A^2\Pi_u \leftarrow X^2\Sigma_g^+$ system of N_2^+

N	P_{11}	P_{12}	Q_{11}	Q_{12}	R_{11}	R_{12}
1			8081.9225 (14)		8090.1324 (−4)	8081.9357 (9)
2	8074.4567 (0)		8082.6684 (−4)	8074.4801 (6)	8094.1642 (−15)	8082.6922 (5)
3	8071.4768 (23)	8063.2937 (−12)	8082.9745 (17)	8071.5065 (−1)	8097.7562 (8)	8083.0064 (15)
4	8068.0506 (18)	8056.5944 (12)	8082.8354 (9)	8068.0922 (22)	8100.9046 (12)	8082.8770 (13)
5	8064.1779 (−30)	8049.4522 (35)	8082.2577 (23)	8064.2291 (−22)	8103.6075 (−39)	8082.3076 (17)
6		8041.8623 (−9)	8081.2393 (16)		8105.8852 (38)	8081.2982 (9)
7	8055.1236 (−23)		8079.7815 (−20)	8055.1921 (−25)	8107.7136 (−20)	8079.8513 (−10)
8	8049.9428 (−2)		8077.8978 (26)	8050.0206 (−3)	8109.1147 (−17)	8077.9760 (30)
9			8075.5732 (−21)		8110.0855 (−7)	8075.6616 (−7)
10	8038.2776 (−15)	8007.1496 (−45)	8072.8290 (25)	8038.3741 (−13)	8110.6272 (−3)	8072.9256 (28)
11		7997.3993 (13)	8069.6535 (19)		8110.7434 (5)	8069.7590 (20)
12		7987.2191 (31)	8066.0505 (−27)		8110.4347 (−3)	8066.1641 (−36)
13		7976.6107 (−4)	8062.0348 (8)		8109.7050 (−12)	8062.1590 (12)
14		7965.5907 (43)	8057.5941 (−27)		8108.5587 (−4)	8057.7264 (−32)
15		7954.1464 (17)	8052.7473 (33)	8001.8125 (−45)	8106.9959 (0)	
16	7993.0968 (−36)	7942.2890 (−4)	8047.4737 (−47)		8105.0185 (−5)	8047.6260 (−36)
17	7984.1171 (27)	7930.0221 (−8)	8041.8023 (1)	7984.2776 (29)	8102.6290 (−17)	
18	7974.7204 (10)	7917.3486 (3)		7974.8919 (30)	8099.8316 (−12)	
19	7964.9181 (2)			7965.0962 (−4)	8096.6258 (−18)	
20	7954.7114 (−11)			7954.8992 (−11)	8093.0162 (−6)	
21	7944.1035 (−16)			7944.2970 (−52)	8089.0026 (4)	
22		7862.6228 (14)	8007.3377 (−44)	7933.3056 (12)	8084.5857 (3)	8007.5441 (−43)
23	7921.6917 (−20)		7999.2497 (14)			
24	7909.8940 (5)		7990.7609 (28)	7910.1178 (−3)	8074.5530 (17)	
25			7981.8753 (24)		8068.9389 (21)	
26			7972.5940 (−4)			
27			7962.9226 (−13)			
28	7858.7737 (25)		7952.8648 (22)		8049.7207 (23)	
29			7942.4121 (3)			
30	7830.8819 (28)					
31			7920.3455 (−9)			
32			7908.7337 (0)			
	P_{21}	P_{22}	Q_{21}	Q_{22}	R_{21}	R_{22}
1	8154.9738 (−5)		8160.1241 (−6)	8154.9881 (1)	8168.6846 (−2)	8160.1355 (−30)
2	8152.6497 (−14)	8147.5365 (−10)	8161.2353 (12)	8152.6737 (−3)	8173.2207 (41)	8161.2588 (18)
3	8150.0246 (−19)	8141.4959 (−27)	8162.0415 (10)	8150.0587 (1)	8177.4443 (5)	8162.0753 (28)
4	8147.0979 (−18)	8135.1602 (18)	8162.5401 (−22)	8147.1395 (−14)		8162.5825 (−10)
5	8143.8684 (−10)	8128.5158 (−6)	8162.7374 (−5)	8143.9201 (3)		8162.7883 (0)
6	8140.3323 (−17)	8121.5728 (18)	8162.6250 (−1)	8140.3932 (−3)		8162.6837 (−10)
7	8136.4887 (−29)	8114.3216 (5)	8162.2045 (28)	8136.5582 (−21)		8162.2735 (31)
8	8132.3385 (−17)	8106.7637 (−9)	8161.4640 (−10)	8132.4169 (−13)		8161.5424 (−5)
9	8127.8774 (−1)	8098.8996 (0)	8160.4125 (1)	8127.9645 (−1)		8160.4999 (4)
10	8123.1010 (0)	8090.7256 (17)	8159.0421 (8)	8123.1970 (−2)		8159.1388 (13)
11	8118.0109 (29)		8157.3490 (3)	8118.1167 (33)		8157.4558 (17)
12	8112.5958 (−3)		8155.3313 (−6)	8112.7124 (17)		8155.4459 (−6)
13	8106.8596 (−30)	8064.3072 (−10)	8152.9894 (12)	8106.9823 (−40)		8153.1127 (9)
14	8100.8072 (25)	8054.8636 (−15)	8150.3155 (9)	8100.9388 (13)		8150.4492 (17)
15	8094.4178 (−22)		8147.3077 (−8)	8094.5603 (−17)		8147.4501 (−4)
16	8087.7064 (6)		8143.9689 (15)	8087.8578 (8)		8144.1210 (24)
17	8080.6610 (12)		8140.2885 (−1)	8080.8206 (4)		8140.4499 (9)
18	8073.2800 (5)		8136.2661 (−38)			8136.4372 (−22)
19	8065.5652 (25)		8131.9077 (−11)	8065.7417 (3)		8132.0857 (−18)
20		7991.3385 (13)	8127.2036 (3)	8057.6916 (−36)		8127.3914 (2)
21		7979.5812 (−21)	8122.1528 (16)	8049.3086 (3)		8122.3511 (29)
22		7967.4934 (26)	8116.7519 (12)	8040.5824 (37)		8116.9581 (13)
23		7955.0594 (13)	8111.0052 (54)			8111.2181 (30)
24			8104.8969 (−1)			8105.1207 (−8)
25		7929.1642 (−8)				8098.6721 (−20)
26		7915.7019 (1)		8002.1959 (−40)		8091.8684 (−33)
27				7991.7339 (15)		8084.7116 (−10)
28						8077.1940 (−17)
29				7969.7444 (35)		8069.3177 (−20)

Table 1 (*continued*)

	P_{21}	P_{22}	Q_{21}	Q_{22}	R_{21}	R_{22}
30		7858.3745 (−3)		7958.2144 (−1)		
31		7843.1683 (−9)				
32		7827.6099 (−21)		7934.0938 (−18)		
33				7921.5014 (2)		

Numbers in the parentheses represent (observed − calculated) $\times 10^4$.

Table 2
Wavenumbers of the observed lines of the (4,4) band of the $A^2\Pi_u \leftarrow X^2\Sigma_g^+$ system of N_2^+

N	P_{11}	P_{12}	Q_{11}	Q_{12}	R_{11}	R_{12}
1			7788.7871 (−10)		7796.9089 (3)	7788.8014 (−3)
2	7781.4014 (−1)		7789.5246 (21)	7781.4241 (−2)	7800.8908 (−9)	7789.5477 (23)
3	7778.4409 (−41)	7770.3568 (3)	7789.8176 (18)	7778.4741 (−29)	7804.4345 (5)	7789.8497 (20)
4	7775.0449 (−25)	7763.7207 (13)	7789.6727 (37)	7775.0891 (6)	7807.5381 (11)	7789.7093 (−8)
5	7771.2105 (4)	7756.6415 (−6)	7789.0851 (11)	7771.2611 (8)	7810.2023 (3)	7789.1347 (5)
6	7766.9341 (−5)	7749.1275 (14)	7788.0633 (8)	7766.9940 (0)	7812.4316 (3)	7788.1225 (7)
7	7762.2231 (3)	7741.1739 (6)	7786.6067 (1)	7762.2918 (4)	7814.2292 (24)	7786.6758 (7)
8	7757.0769 (−3)	7732.7848 (−12)	7784.7165 (−23)	7757.1554 (5)	7815.5901 (−8)	7784.7937 (−27)
9	7751.4985 (−15)	7723.9696 (30)	7782.4003 (−12)	7751.5854 (−14)	7816.5250 (−7)	7782.4871 (−11)
10	7745.4945 (7)	7714.7197 (21)	7779.6577 (7)	7745.5909 (11)	7817.0323 (−16)	7779.7532 (2)
11	7739.0621 (9)	7705.0419 (−1)	7776.4881 (−3)	7739.1675 (13)	7817.1163 (−15)	7776.5927 (−7)
12	7732.2037 (−13)	7694.9434 (10)	7772.8992 (13)	7732.3180 (−11)	7816.7785 (−15)	7773.0118 (−3)
13	7724.9273 (−5)		7768.8877 (−7)	7725.0503 (−9)	7816.0211 (−17)	7769.0108 (−10)
14	7717.2333 (7)		7764.4630 (6)	7717.3652 (2)	7814.8495 (8)	7764.5957 (8)
15	7709.1219 (0)		7759.6221 (−4)	7709.2640 (4)	7813.2624 (24)	7759.7627 (−14)
16	7700.5986 (0)		7754.3707 (−4)	7700.7490 (−3)	7811.2573 (−16)	
17			7748.7112 (6)		7808.8471 (−5)	7748.8706 (1)
18			7742.6427 (−6)		7806.0264 (−17)	7742.8119 (−5)
19			7736.1693 (−22)		7802.8042 (19)	
20			7729.2970 (−1)		7799.1727 (5)	7729.4830 (−14)
21			7722.0207 (−15)		7795.1390 (−3)	7722.2198 (12)
22			7714.3486 (1)		7790.7054 (0)	7714.5552 (10)
23			7706.2773 (−8)		7785.8712 (−8)	
24			7697.8117 (−6)		7780.6393 (−11)	
25					7775.0078 (−42)	
26					7768.9876 (−5)	
27					7762.5712 (15)	
28					7755.7595 (14)	
29					7748.5572 (31)	
30					7740.9623 (36)	
	P_{21}	P_{22}	Q_{21}	Q_{22}	R_{21}	R_{22}
1			7866.9400 (5)	7861.8567 (−48)	7875.4010 (14)	
2		7854.4884 (−8)	7868.0265 (−14)	7859.5659 (1)	7879.8708 (2)	7868.0511 (3)
3	7856.9372 (12)	7848.5111 (32)	7868.8136 (8)		7884.0368 (2)	7868.8431 (−17)
4	7854.0234 (−29)	7842.2228 (−20)	7869.2921 (−6)	7854.0654 (−21)		7869.3311 (−27)
5	7850.8117 (−10)	7835.6389 (−2)	7869.4655 (−3)	7850.8619 (−9)	7891.4495 (34)	7869.5156 (−5)
6	7847.2925 (−9)	7828.7509 (12)	7869.3311 (10)	7847.3520 (−9)	7894.6859 (7)	7869.3900 (5)
7	7843.4665 (−4)	7821.5591 (40)	7868.8868 (32)	7843.5359 (5)		7868.9546 (26)
8	7839.3291 (−20)	7814.0558 (21)	7868.1231 (−3)	7839.4077 (−11)	7900.2200 (3)	7868.2013 (2)
9	7834.8815 (−23)	7806.2422 (−13)	7867.0475 (2)	7834.9682 (−24)	7902.5082 (−13)	7867.1345 (3)
10	7830.1227 (1)	7798.1205 (−18)	7865.6512 (−15)	7830.2189 (3)	7904.4771 (−5)	7865.7475 (−11)
11	7825.0429 (−22)		7863.9378 (12)	7825.1489 (−12)	7906.1185 (−23)	7864.0424 (8)
12	7819.6454 (−32)	7780.9379 (0)	7861.8978 (14)	7819.7614 (−14)	7907.4372 (9)	7862.0120 (13)
13	7813.9329 (20)	7771.8707 (7)		7814.0558 (17)	7908.4201 (−15)	7859.6535 (6)
14	7807.8901 (11)	7762.4819 (4)	7856.8360 (29)	7808.0221 (7)	7909.0751 (16)	7856.9696 (40)
15	7801.5230 (24)	7752.7683 (−20)	7853.8040 (−6)	7801.6643 (20)	7909.3896 (0)	7853.9461 (−1)
16	7794.8232 (−2)	7742.7345 (7)	7850.4426 (12)	7794.9733 (−9)	7909.3670 (−3)	7850.5934 (12)
17	7787.7951 (3)	7732.3688 (−9)	7846.7423 (12)	7787.9550 (3)	7909.0075 (36)	7846.9028 (18)
18	7780.4316 (−9)	7721.6760 (3)	7842.7019 (4)	7780.6007 (−8)	7908.2966 (−8)	7842.8705 (0)
19		7710.6508 (10)	7838.3190 (−11)			7838.4971 (−12)

Table 2 (*continued*)

	P_{21}	P_{22}	Q_{21}	Q_{22}	R_{21}	R_{22}
20	7764.6989 (5)	7699.2904 (6)	7833.5948 (−1)	7764.8855 (−1)		7833.7809 (−13)
21	7756.3199 (−25)		7828.5251 (11)	7756.5170 (−18)		7828.7214 (10)
22	7747.6092 (46)		7823.1048 (−5)	7747.8113 (11)		7823.3107 (−1)
23			7817.3368 (−3)	7738.7579 (−1)		7817.5534 (16)
24	7729.1381 (13)		7811.2154 (−23)	7729.3605 (−1)		7811.4407 (−8)
25				7719.6168 (4)		7804.9808 (22)
26			7797.9176 (−15)	7709.5237 (−4)		
27						
28						7783.4560 (−25)
29						7773.5661 (−44)

Numbers in the parentheses represent (observed − calculated) $\times 10^4$.

coupling constant, A_v, the centrifugal distortion of the spin–orbit constant, A_{Jv}, and the lambda doubling constants, p_v and q_v, in addition to the constants mentioned above. The molecular parameters, $\gamma_{v'}$ and $A_{Jv'}$, in the $^2\Pi$ state have been shown to be highly correlated [25] and $\gamma_{v'}$ was constrained to zero. For the initial assignment of the (3,3) band, molecular constants from Radunsky and Saykally's (7,3) band and the constants for the $v' = 3$ from Miller et al. were used [7,10]. The (4,4) band was calculated from the constants of the (4,0) band from Miller et al. and the (7,4) band from Chen et al. [7,20]. The $T_{v'v''}$ values were determined from the vibrational equilibrium constant of Royen and coworkers [18]. The deviation of the measured lines from the predicted values had a maximum value and an rms value of 0.042 and 0.023 cm^{-1} for the (3,3) band and 0.058 and 0.009 cm^{-1} for the (4,4) band, respectively.

Among the lines we have observed, 236 lines were identified to the (3,3) band up to $J = 32.5$ and 242 lines to the (4,4) band up to $J = 30.5$. These lines are listed in Tables 1 and 2. Fig. 3 shows the Fortrat plot for the (4,4) band of the A–X system and the corresponding stick spectrum. From the plot, the characteristic features of a $^2\Pi \leftarrow {}^2\Sigma$ transition, where the $^2\Pi$ state is Hund's

Table 3
Molecular parameters (in cm^{-1}) of the (3,3) and (4,4) bands of the $A^2\Pi_u \leftarrow X^2\Sigma_g^+$ system of N_2^+

	$A^2\Pi_u$				
	$v = 3$			$v = 4$	
	Ref. [19]	Ref. [7]	This work	Ref. [7]	This work
$T_{v'v''}$			8119.71996(23)[a]		7826.57863(19)
$B_{v'}$	1.678321(21)	1.678385(28)	1.678413(11)	1.659380(31)	1.659406(10)
$D_{v'} \times 10^6$	5.882(22)	5.890(45)	5.936(10)	5.947(83)	5.968(18)
$A_{v'}$	−74.62533(88)	−74.5895(58)	−74.62560(40)	−74.61103(84)	−74.61571(31)
$A_{Jv'} \times 10^5$	−0.352(17)	−8.55(1.00)	−3.681(69)	−5.325(295)	−3.802(65)
$p_{v'} \times 10^3$	5.487(57)	5.31(39)	5.406(32)	5.891(84)	5.857(29)
$q_{v'} \times 10^4$	−3.607(23)	−3.83(17)	−3.560(12)	−3.969(79)	−3.837(19)
J_{max}/N_{max}	30		32.5	20.5	30.5
Number of lines	207		236	173	242
Δv[b]	0.007		0.005	0.004	0.005
rms	0.0035		0.0019	0.0034	0.0015
Band	A–X (3,1)		A–X (3,3)	A–X (4,0)	A–X (4,4)

	$X^2\Sigma_g^+$						
	$v = 3$			$v = 4$			
	Ref. [10]	Ref. [16]	This work	Ref. [20]	Ref. [19]	Ref. [15]	This work
$B_{v''}$	1.865015(41)	1.864977(20)	1.864995(10)	1.845440(21)	1.845600(37)	1.845478(43)	1.845524(11)
$D_{v''} \times 10^6$	6.039(68)	6.015(31)	6.029(9)	5.942(27)	6.162(47)	5.923(82)	6.074(20)
$\gamma_{v''} \times 10^3$	9.257(73)	9.205(39)	9.164(10)	9.187(47)	9.98(11)	9.244(79)	9.137(11)
J_{max}/N_{max}		28	32.5	32.5	34	25.5	30.5
Number of lines	185	244	236	272	237	193	242
Δv	0.003	0.007	0.005	0.007	0.007	0.005	0.005
rms	0.00599		0.0019	0.0058	0.0052	0.0042	0.0015
Band	A–X (7,3)	A–X (6,3)	A–X (3,3)	A–X (7,4)	A–X (7,4)	A–X (9,4)	A–X (4,4)

[a] The numbers in the parentheses represent one standard deviation for the last digits.
[b] Reported accuracy.

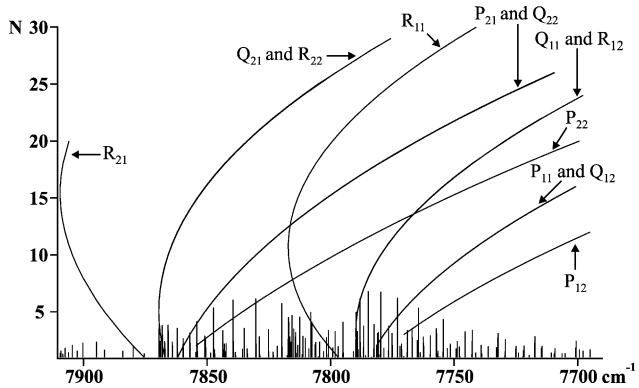

Fig. 3. Fortrat plot of the (4,4) band of the $A^2\Pi_u \leftarrow X^2\Sigma_g^+$ system of N_2^+ and the corresponding stick spectrum. The stick spectrum was derived from the experimentally determined values of the line positions and the calculated intensities from the rotational temperature measurements (see below).

case (a), are seen with 6 subbands on each side of the band origin resulting from the transitions to the two spin–orbit states. Resolution of all the subbands in the Fortrat plot is not possible due to the small value for the spin-rotation constant. A similiar plot was obtained for the (3,3) band. After the assignment of the (3,3) and (4,4) bands, nearly 100 lines were left unassigned. These lines are believed to belong to the (10,9) and (11,10) vibrational bands of the Meinel system; however, a definite assignment has not been made.

4. Analysis

The (3,3) and (4,4) bands were fit using a non-linear least-squares routine and the Hamiltonians described above. The fits did not produce accurate results for the spin-rotation constants. The parameters in the model are highly correlated in the fitting routine. Combination differences were taken to isolate the spin-rotation constant from the rest of the parameters. The combination differences between the following subbands were used: R_{22} and Q_{21}, Q_{22} and P_{21}, R_{12} and Q_{11}, and Q_{12} and P_{11}. When these combination differences were plotted against the quantum number N, a linear plot was obtained with the slope equal to the spin-rotation constant. The non-linear least-squares fit was then redone holding

Table 4
Deslandres table of band origins (in cm^{-1}) for the $A^2\Pi_u \leftarrow X^2\Sigma_g^+$ system of N_2^+

v'	v''						
	0	1	2	3	4	5	6
0	**9015.9990(7)**[a,b,c]	**6841.2492(−3)**[c]	4699.0099	2589.5368	513.0876	−1530.0804	−3539.7099
1	**10889.4527(−53)**[c]	8714.7091	**6572.4716(21)**[c]	4462.9964	2386.5473	343.3793	−1666.2502
2	**12732.8463(33)**[d]	10558.0942	8415.8545	6306.3815	4229.9323	**2186.7676(33)**[e]	177.1348
3	14546.1795	**12371.42691(−376)**[f]	10229.1910	**8119.71996(199)**[g]	6043.2688	4000.1008	1990.4713
4	**16329.4901(−31)**[h]	14154.7443	12012.5047	9903.0316	**7826.57863(−380)**[g]	5783.4144	3773.7850
5	**18082.8154(64)**[i]	15908.0602	13765.8206	11656.3475	9579.8983	7536.7303	5527.1008
6	19806.1518	17631.4030	15489.1634	**13379.68843(−186)**[j]	11303.2411	9260.0731	7250.4436
7	21499.5457	19324.7969	**17182.55382(−342)**[k]	**15073.0864(22)**[l]	**12966.63636(136)** [f]	10953.4670	8943.8375
8	23163.0144	20988.2655	18846.0259	**16736.5579(50)**[m]	14660.1037	**12616.93160 (−408)**[f]	10607.3062
9	24796.5811	22621.8322	20479.5926	18370.1195	**16293.6702(−1)**[n]	14250.5023	12240.8729
10	26400.2684	24225.5196	22083.2799	19973.8069	17897.3577	15854.1897	13844.5602
11	27974.0987	25799.3499	23657.1102	21547.6372	19471.1880	**17428.01777 (−225)**[o]	15418.3905
12	29518.0937	27343.3449	25201.1053	23091.6322	21015.1830	18972.0150	**16962.38782(228)**[o]
13	31032.2747	28857.5258	26715.2862	24605.8132	22529.3640	20486.1960	**18476.5659(−6)**[p]

[a] Bold-faced numbers are experimentally determined values, whereas the other values have been calculated from Table 5.
[b] The numbers in the parenthesis represent observed − calculated and apply to the last digits.
[c] Ref. [26].
[d] Ref. [27].
[e] Ref. [14].
[f] Ref. [19].
[g] This work.
[h] Ref. [7].
[i] Ref. [28].
[j] Ref. [16].
[k] Ref. [20].
[l] Ref. [10].
[m] Ref. [13].
[n] Ref. [15].
[o] Ref. [29].
[p] Ref. [11].

γ constant at the value determined from the combination differences. The molecular constants are presented in Table 3 and are compared to previous experimental results. The rms error of the fit for the (3,3) and (4,4) bands are 0.0019 and 0.0015, which is better than the accuracy of the experimental error. The $^2\Pi$ centrifugal correction to the spin–orbit interaction, $A_{Jv'}$, used here differs from the one used by Miller et al. and Collet et al. They report A_{Dv}, whereas we report A_{Jv}, and the difference between the two values is a factor of 1/2 [7,19]. Their values have been adjusted accordingly for comparison in Table 3. It should be noted that the centrifugal correction to the spin–orbit interaction varies significantly among the reported results.

Using our results together with the previous studies of higher vibrational states of the A–X system of N_2^+, a Deslandres table was produced, as shown in Table 4. The bold faced elements in the table are experimentally determined values of $T_{v'v''}$. In making the Deslandres table, experimental values of $T_{v'v''}$ were used whose accuracy is clearly stated. The reported values of $T_{v'v''}$ obtained from fits, where some molecular parameters were held constant during the fitting routine, were excluded from the table. Additionally, values of $T_{v'v''}$, based on wavenumber measurements with high uncertainty, were also excluded from the table. A higher vibrational band, the (15,8) band, has been reported in literature, however, this was not included in the table for reasons described above. From this table, a global fit of the $T_{v'v''}$ values was done to obtain the equilibrium vibrational constants in Table 5.

The rotational temperature was determined by generating Boltzmann plots for the (3,3) and (4,4) bands. The functional form used in the fit was

$$I \propto g_I S |R_{v'v''}|^2 e^{-E''_{\mathrm{Rot}}/kT_{\mathrm{Rot}}},$$

where I is the intensity, g_I is the degeneracy as a result of the nuclear spin statistics, S is the line strength, and $|R_{v'v''}|^2$ is the Franck–Condon factor. The line strengths were determined from the formula of Earls [30] using an intermediate Hund's case and the Franck–Condon factors were from [31]. The rotational temperatures were determined to be 407 ± 35 and 400 ± 31 K for the (3,3) and (4,4) bands, respectively, where the uncertainty represents three standard deviations. The Boltzmann plots are shown in Fig. 4.

Table 5
Molecular equilibrium constants (in cm^{-1}) of the $X^2\Sigma_g^+$ and the $A^2\Pi_u$ states of N_2^+

	$X^2\Sigma_g^+$	$A^2\Pi_u$
T_e	0	9167.4672(58)
ω_e	2207.0115(60)[a]	1903.5598(46)
$\omega_e x_e$	16.0616(23)	15.0573(14)
$\omega_e y_e$	−0.04289(25)	0.00451(16)
$\omega_e z_e \times 10^5$		−2.02(60)
rms error = 0.0032		

[a] The numbers in the parentheses represent one standard deviation for the last digits.

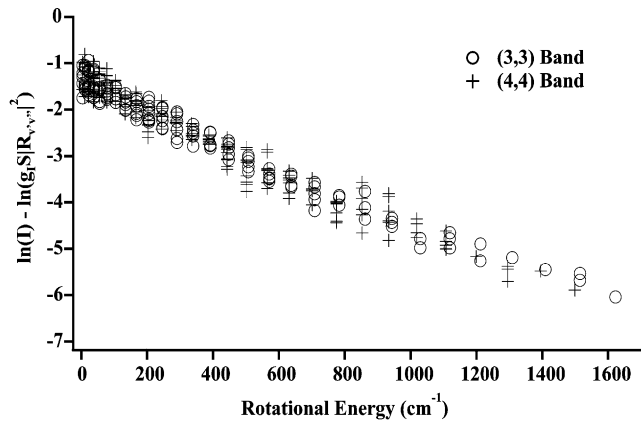

Fig. 4. Boltzmann plots for the (3,3) and (4,4) bands of the $A^2\Pi_u \leftarrow X^2\Sigma_g^+$ system of N_2^+.

Acknowledgments

We thank Guy Guelachvili for supplying us with the reference spectrum of NH_3. This work was supported by NSF Grant PHYS 00-99442.

References

[1] W.H.J. Childs, Proc. R. Soc. London A 137 (1932) 641–661.
[2] A.B. Meinel, Astrophys. J. 112 (1950) 562–563.
[3] A.B. Meinel, Astrophys. J. 114 (1951) 431–437.
[4] F.W. Dalby, A.E. Douglas, Phys. Rev. 84 (1951) 843.
[5] A.E. Douglas, Astrophys. J. 117 (1953) 380–386.
[6] W. Benesch, D. Rivers, J. Moore, J. Opt. Soc. Am. 70 (1980) 792–799.
[7] T.A. Miller, T. Suzuki, E. Hirota, J. Chem. Phys. 80 (1984) 4671–4678.
[8] C.S. Gudeman, M.H. Begemann, J. Pfaff, R.J. Saykally, Phys. Rev. Lett. 50 (1983) 727–731.
[9] C.S. Gudeman, R.J. Saykally, Annu. Rev. Phys. Chem. 35 (1984) 387–418.
[10] M.B. Radunsky, R.J. Saykally, J. Chem. Phys. 87 (1987) 898–901.
[11] D.T. Cramb, A.G. Adam, D.M. Steunenberg, A.J. Merer, M.C.L. Gerry, J. Mol. Spectrosc. 141 (1990) 281–289.
[12] D.T. Cramb, M.C.L. Gerry, F.W. Dalby, I. Ozier, Chem. Phys. Lett. 178 (1991) 115–120.
[13] B. Lindgren, P. Royen, M. Zackrisson, J. Mol. Spectrosc. 146 (1991) 343–350.
[14] W.C. Ho, W. Jäger, D.T. Cramb, I. Ozier, M.C.L. Gerry, J. Mol. Spectrosc. 153 (1992) 692–700.
[15] B. Lindgren, P. Royen, M. Zackrisson, J. Mol. Spectrosc. 156 (1992) 319–326.
[16] I. Hadj Bachir, T.R. Huet, J.L. Destombes, J. Mol. Spectrosc. 170 (1995) 601–603.
[17] A. Al-Khalili, H. Ludwigs, P. Royen, J. Mol. Spectrosc. 183 (1997) 200–203.
[18] A. Al-Khalili, H. Ludwigs, P. Royen, Chem. Phys. Lett. 284 (1998) 191–194.

[19] D. Collet, J.L. Destombes, I. Hadj Bachir, T.R. Huet, Chem. Phys. Lett. 286 (1998) 311–316.
[20] Y. Liu, C. Duan, S. Wu, H. Zhuang, Y. Chen, J. Mol. Spectrosc. 208 (2001) 144–147.
[21] B.J. McCall, T. Oka, J. Chem. Phys. 113 (2000) 3104–3110.
[22] C.M. Lindsay, E.T. White, T. Oka, Chem. Phys. Lett. 328 (2000) 129–134.
[23] G. Guelachvili (private communication).
[24] Y. Endo, S. Saito, E. Hirota, J. Mol. Spectrosc. 92 (1982) 443–450.
[25] J.M. Brown, J.K.G. Watson, J. Mol. Spectrosc. 65 (1977) 65–74.
[26] D.W. Ferguson, K.N. Rao, P.A. Martin, G. Guelachvili, J. Mol. Spectrosc. 153 (1992) 599–609.
[27] I. Hadj Bachir, H. Bolvin, C. Demuynck, J.L. Destombes, A. Zellagui, J. Mol. Spectrosc. 166 (1994) 88–96.
[28] C.H. Kuo, I.W. Milkman, T.C. Steimle, J.Y. Moseley, J. Chem. Phys. 85 (1986) 4269–4275.
[29] S. Wu, Y. Chen, H. Zhuang, X. Yang, Z. Bi, L. Ma, Y. Lu, J. Mol. Spectrosc. 209 (2001) 133–135.
[30] L.T. Earls, Phys. Rev. 48 (1935) 423–424.
[31] F.R. Gilmore, R.R. Laher, P.J. Espy, J. Phys. Chem. Ref. Data 21 (1992) 1005–1107.